Molecular Motions of Hydrogen Bonded CH_3CN in the Zeolite Chabazite: Comparison of First-Principles Molecular Dynamics Simulations with Results from ^1H, ^2H, and ^{13}C NMR

B. L. Trout,[†] B. H. Suits,[‡] R. J. Gorte,[§] and David White*[,||]

Department of Chemical Engineering, Massachusetts Institute of Technology, Cambridge, Massachusetts 02139, Department of Physics, Michigan Technological University, Houghton, Michigan 49931, Department of Chemical Engineering and Department of Chemistry, University of Pennsylvania, Philadelphia, Pennsylvania 19104

Received: August 8, 2000; In Final Form: October 17, 2000

Density functional theory calculations with periodic boundary conditions, Car−Parrinello simulations, and multinuclear solid-state NMR experiments at temperatures in the range 77 to 450 K, have been performed to probe the structure and motion of acetonitrile adsorbed at an isolated Brønsted-acid site in chabazite. The 1:1 stoichiometric acetonitrile adsorption complex is hydrogen-bonded to the acid site, and two minima have been found for the position of adsorbed acetonitrile on a proton associated with a single oxygen atom in the zeolite lattice. In agreement with experiment, the results of the Car−Parrinello simulations indicate a free rotation of the methyl group protons about the acetonitrile molecular axis, as well as a motion of this axis that can be described as a two-dimensional libration about the hydrogen bond. The details and temperature dependence of the distributions describing the librational amplitudes as a function of temperature derived from the simulations are, however, not in agreement with experiment. Whereas the experimental distributions reach a limiting value at 300 K, the amplitudes continuously increase in the simulations. The reasons for this are briefly discussed.

1. Introduction

An important aspect influencing catalytic properties of solid acid zeolites is the interaction of adsorbates with the framework around the acid site. In many catalytic processes, the first step is the formation of a hydrogen-bonded adsorption complex, especially with such weak bases as alcohols, ketones, aldehydes, etc.[1−3] While differences in the properties of such adsorption complexes in specific zeolite structures may be attributable in part to some differences in intrinsic proton affinities of the adsorbates,[4] the rates and selectivities of the thermally activated reactions, determined by the energy and entropy of transition states and hence the structure of the transition states, are highly sensitive to the interactions between adsorbates and the zeolitic framework. The time scale of these interactions, often in the picosecond and subpicosecond range, is modulated by the nature of the confinement of the adsorbed molecule in the zeolite or, more specifically, by the adsorbed molecule−framework interactions. Thus, it is not unreasonable to expect framework topology to play a role in the catalytic activity. Important questions then are what are the nature and magnitude of these topologically sensitive interactions as manifested by the molecular motions, and how well can this dynamics be described in present day theoretical calculations employed in computer simulations modeling reaction pathways for the purpose of basic understanding as well the more practical catalyst design.

For weak bases such as acetone and acetonitrile, a significant part of the stabilization of the 1:1 stoichiometric adsorption complex involves the formation of a hydrogen bond at the Brønsted site.[5−8] Additional stabilization arises from the local host−guest electrostatic and van der Waals interactions in the zeolite cavity (confinement effect),[9] and a longer range contribution from the extended lattice, often referred to as the embedding effect.[10−13] All of these interactions are dependent on the zeolite framework topology and structural relaxation. An approximate measure of the total stabilization energy attributable to the topology sensitive confinement and embedding interactions in the case of a base adsorbed in the zeolite ZSM5 (H-MFI), can be obtained by comparing the magnitudes of the differential heat of adsorption in H-MFI, with that of the completely siliceous material, silicalite, at loadings corresponding to one molecule per acid site. For the acetone adsorption complex, it is approximately 50% or 60 kJ/mol at 0 K.[3] Admittedly, there are several important assumptions implied in this comparison, such as identical site occupation in the two zeolites, neglect of effects due to structural relaxation which will not be the same in both zeolites, etc. As a result, this fraction probably represents an upper limit. Nevertheless, the magnitude of this fraction of the total bonding energy is not surprising given the partially ionic character of the zeolite framework.

Another approach to the understanding of adsorbed molecule−framework interactions has been the use of theoretical modeling. Most of the early studies have been restricted to ab initio cluster model calculations in which the zeolite acid site is simulated by a small fragment, typically two, three, or four tetrahedral sites. The framework, treated classically, can be introduced by artificial point charge fields containing the cluster to emulate the longer range forces of the electrostatic potential of the zeolite cavity.[8−11] This procedure, however, often introduces errors of the same order as neglecting the framework. Alternatives introduced by Sauer and co-workers[12a,b] and Warshel et al.,[12b] are to perform simultaneously coupled classical and quantum

* Corresponding author.
[†] Massachusetts Institute of Technology.
[‡] Michigan Technological University.
[§] Department of Chemical Engineering, University of Pennsylvania.
[||] Department of Chemistry, University of Pennsylvania.

10.1021/jp0028204 CCC: $19.00
Published on Web 11/17/2000

mechanical calculations or to use the empirical valence bond approach. These methods do not suffer from the same problems as the previous one. The first case is tedious to set up and has not been tested for complex reactions that may involve specific interactions with the zeolite framework, and the latter case depends on the availability of empirical data. More recent calculations using "first-principles" techniques and periodic boundary conditions with full zeolite topology, have clearly demonstrated the importance of the role of the lattice in the adsorption process.[14−18] These display the effects of different zeolite environments not only in the optimized static structures and energetics of the stable adsorption complex but, in conjunction with molecular dynamics simulations, also dynamical effects such as molecular motions and energy transfer within the adsorption complex at finite temperatures.[19] Dynamical effects are especially important because the temperature dependence of such dynamics, governed by the molecule−framework interactions specific to a given topology, provides another means of experimentally verifying the validity of models employed in the simulations.

In principle such experiments can be done using both transient-optical[20] and solid-state NMR spectroscopic studies.[21,22] Unfortunately, except in special cases,[23−26] the more direct optical studies are not readily adaptable to the study of reactive adsorbates in powdered solid acids. On the other hand, NMR studies provide useful but dynamically averaged information when the time scales of the NMR interactions are very long compared to the time scales of the molecular motions.[21,22] We have recently demonstrated in a solid-state NMR investigation of the localized hydrogen-bonded, acetonitrile−MFI adsorption complex that it is possible to observe temperature-dependent line shapes resulting from the excitation of the libration of the molecular axis of the adsorbed molecule in the framework cavity.[22] Since the librational frequency is on the order of a few wavenumbers, this experiment provided only dynamically averaged information relating to root-mean-square amplitudes that describe the statistics of the molecular reorientations on thermal excitation.[22] Unfortunately, because of the large size of the H-MFI unit cell (288 atoms per unit cell, 12 different T sites) and limitations imposed by the available computational facilities, it was not possible to compare results from our NMR studies of the molecular motions of the hydrogen-bonded CH_3-CN−H−MFI adsorption complex[22] with theoretical simulations based on "first principles".

In this paper we present both a "first-principles" theoretical and experimental NMR studies of the molecular motions of the 1:1, stoichiometric, acetonitrile adsorption complex in the zeolite chabazite (H−CHA) designated CHA in this paper, over a range of temperatures. We have employed a high-silica (Si/Al ratio of 40) CHA (36 atoms per unit cell) sample containing on the average one acid site per unit cell for the experimental NMR studies to avoid interactions of molecules adsorbed in adjacent sites. For the theoretical study, we have used a model consisting of one unit cell with periodic boundary conditions. In this model there is one acid site per unit cell; and, since the lattice constants are approximately 10 Å, we are simulating essentially isolated acid sites. Such an approach leads to a meaningful comparison between theory and experiment. In the next section we present the model and methodology employed in the "first principles" theoretical simulations along with results relating to the optimized static structure, energetics, and molecular motions of the adsorption complex as a function of temperature derived from the molecular dynamics. This is followed by an experimental characterization of the CHA sample, temperature programmed desorption (TPD), and calorimetric studies of the acetonitrile adsorption complex, and presentation of the molecular motions of the complex derived from the multinuclear, solid-state, NMR, temperature-dependent line shapes. Finally results from both theory and experiment are compared. We will show that while the simulations go a long way toward explaining the experimental results qualitatively, and even semiquantatively, and may provide insights not directly available from experiments, there are still significant discrepancies between the two even for this simple zeolite.

2. Theoretical Calculations

2.1. Model and Methodology. CHA was chosen as the zeolite to study primarily because it has a small unit cell size and because it is of commercial interest.[27,28] The unit cell consists of 36 atoms (12 T, 24 O) and can thus be studied with reasonable computational expense using quantum mechanical density-functional theory with a plane-wave basis set and periodic boundary conditions. For the calculations described below, an infinite crystal of CHA has been modeled by choosing experimentally determined unit-cell parameters and atomic positions and repeating this system ad infinitum using periodic boundary conditions. Specifically, plane-wave basis sets have been used with a cutoff of 55 Ry. The initial geometry, lattice parameters, and lattice space group were obtained from Smith et al.[27] Troullier−Martins pseudopotentials[29] have been used to describe the core electrons, and the PW91 functional has been used for the exchange and correlation functional.[30] This methodology has been previously validated and is similar to that used by several other researchers.[16−19,31−37] One Si site was substituted for an Al site, and a proton was added, bonded to the O atom which yields the strongest OH bond and is adjacent to the Al atom.[16] First, a geometry optimization was performed on the acetonitrile, hydrogen-bonded to the H site. The results of this static calculation are presented in section 2.2. Next, Car−Parrinello simulations[38] were performed using a time step of 7.0 au (0.17 fs). To determine properties averaged within the canonical ensemble, a Nosé−Hoover chain thermostat with a length of 4 and a characteristic frequency of 500 cm^{-1} was used on the nuclear degrees of freedom.[39−41] Three simulations were performed, at 77, 300, and 450 K. The systems were equilibrated for 0.5 ps, and properties were averaged for 4.5 ps. This equilibration period was sufficient for the ionic kinetic energies and the Kohn−Sham energies to begin fluctuating around average values. The code used was CPMD.[42] The results and analysis of the dynamic simulations are presented in section 2.3 below. Further calculations of the hopping of the adsorbate across the CHA eight-membered ring are presented in section 2.4.

2.2. Structure of Adsorbed Complex and Binding Energy. Two static structures were found with almost equal energies of adsorption of the acetonitrile. The first called "position 1", provided the initial structure for the Car−Parrinello simulations. This static hydrogen bonded structure of the adsorbed molecule in the vicinity of the eight-membered ring of the CHA zeolite containing one acid site per unit cell is shown in Figure 1. The second, "position 2", is almost a mirror image on the opposite side of the ring. The possibility of a second structure became apparent while attempting an interpration of the NMR line shapes based on both the experimental results and the Car−Parrinello simulations. It should be noted that during the Car−Parrinello simulations described below, the acetonitrile molecule remained on the same side of the eight-membered ring (position 1). We also note that studies on cluster models, which do not

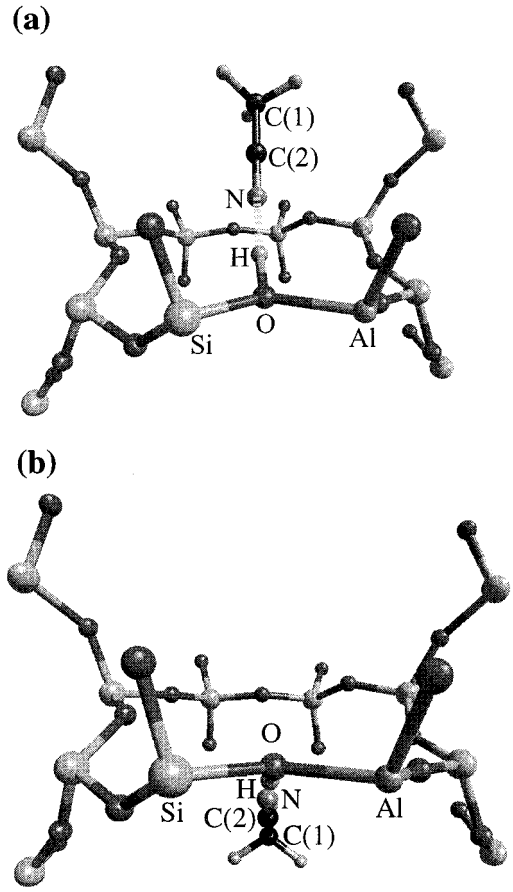

Figure 1. Geometry of optimized structures of acetonitrile adsorbed at an acid site in chabazite (H−CHA). (a) Position 1, P1. (b) Position 2, P2.

treat the zeolite lattice, have shown that there is only one stable position for the proton on the oxygen atom.[43] This result would also lead one to believe that there would be only one stable position for any adsorbate at the acid site. However, when the ring of the zeolite is included in the model, we find there are at least two stable positions for the acetonitrile adsorbed at the acid site. In Table 1, the structural and energetic properties of the hydrogen bonded acetonitrile in both position 1 and position 2 in CHA are presented.

Our calculated energy of adsorption at 0 K for position 1, corresponding to a loading of one molecule of CH_3CN per unit cell to form the 1:1 stoichiometric hydrogen bonded adsorption complex, is −68.4 kJ/mol. Other studies performed on cluster models of the zeolite have yielded energies of adsorption of between 44 and 56 kJ/mol.[5,7,44,45] We have measured via microcalorimetry the enthalpy of adsorption of CH_3CN at 400 K of -100 ± 5 kJ/mol (see section 3 below). Assuming that the ideal gas equation of state is valid and ignoring nonzero temperature vibrational contributions, $\Delta U_{ads}^{0\ K} = \Delta H_{ads}^{400\ K} + 4R(400\ K)$. This yields a measured internal energy of adsorption at 0 K of -87 ± 5 kJ/mol. Finally, assuming that the net change in zero-point energy of vibrational contributions for adsorption are 8 kJ/mol, a typical value found for adsorption of bases on zeolitc acid sites,[46] then the calculated internal energy of adsorption at 0 K is −60.4 kJ/mol. For position 2, a similar calculation would lead to an internal energy of adsorption at 0 K of −64.1 kJ/mol. The discrepancy between calculated and measured internal energy of adsorption of CH_3CN is thus $23-27 \pm 5$ kJ/mol. It is primarily a result of errors in the exchange-correlation terms of the density functional used, in particular the inadequate treatment of London dispersion forces by current density functionals. We, however, estimate that the contribution to the energy of interaction between the adsorbate and the rest of the lattice due to London dispersion forces will be of the order of 20 kJ/mol. The effect of these errors on the computed properties other than the binding energy of CH_3CN is uncertain, and in fact, only direct comparison between the results of simulations and experiment can provide the necessary insights. In section 4 we make, as best we can, this comparison with results derived from NMR experiments.

The calculated geometry, Table 1, shows that the C−C−N structure of the acetonitrile-CHA adsorption complex is almost linear, and the adsorbed molecule is bound to the acid site with a short hydrogen bond of 1.56 Å. As in the ab initio cluster model calculations,[5,7,44,45] proton transfer to the adsorbate does not occur. The important difference between our calculated geometry and that of a full optimization at the HF//6-31G* level for a $H_3SiOHAlH_2OSiH_3$ cluster,[5] in which the dangling bonds are saturated with hydrogen atoms (column 3, Table 1), lies in the shorter H−O bond and longer N−H bond. This is consistent with a weaker hydrogen bond and the smaller adsorption energy, resulting from the large structural relaxation of the cluster. A similar result for a smaller cluster size was also obtained by Florián and Kubelková,[7] who found an N−H distance of 1.955 Å using HF/6-31G* with a cluster model without geometry constraints. Recently, Blaszkowski and van Santen found an N−H bond length of 1.73 Å using DFT/B3LYP and mixed basis set, primarily consisting of double-ζ,[46] and no constraints in their calculations.

A stronger hydrogen bond can, however, be obtained in cluster calculations by imposing artificial constraints in the energy optimization of the adsorption complex that maintain bond lengths and angles more closely to that of the known zeolite structure.[44,47] This is illustrated in column 4 of Table 1, where in optimizing the total energy of a cluster similar in size to that of column 3 (except hydroxyl groups instead of hydrogen atoms saturate the dangling bonds) at the level of HF/double-ζ, only the two bridging oxygens are allowed to relax.[44]

2.3. Librational Motion of the H-bonded Adsorption Complex via First-Principles Molecular Dynamics. Car−Parrinello simulations of the acetonitrile adsorbed at the acid site in the CHA zeolite framework were performed at simulation temperatures of 77, 300, and 450 K. We emphasize that, because of the approximate nature of the quantum mechanical method used in these calculations, the simulation temperatures cannot be expected to exactly match experimental temperatures, nor can they be easily related to the experimental values by some simple scaling factor. In Table 2, average structural parameters obtained from the simulations for the molecule at position 1 at the above temperatures, along with the standard deviations, are given together with values of the optimized structure. For all of the simulations, the molecule remained hydrogen bonded to the acid site of CHA, though it is clear from the standard deviations that the hydrogen bond becomes significantly stretched and bent at the higher temperatures. Further, the protons in the methyl group exhibited free rotation about the molecular axis at all temperatures. Although no simulations were attempted for position 2 of the adsorbed molecule, the fact that it is essentially a mirror image of position 1 would suggest a similar behavior at all simulation temperatures.

In the first three rows of Table 3, several structural parameters relating the orientation of the acetonitrile molecule relative to the eight-membered ring (shown in Figure 1) at the three simulation temperatures are compared for the optimized static

TABLE 1: Energetic and Structural Parameters of Adsorbed Acetonitrile in CHA

property[a]	PW-91 (this study) periodic model position 1 (P1)	PW-91 (this study) periodic model position 2 (P2)	HF/6−31G*[5] cluster model, no geometry constraint	HF-double ζ[43] cluster model with geometry constraint
acetonitrile binding energy (kJ/mol)	68.4	72.1	44.0	56.0
C(1)−C(2) bond	1.45	1.44	1.47	1.48
C(2)−N bond	1.16	1.16	1.13	1.15
N−H bond	1.56	1.48	1.95	1.56
H−O bond	1.06	1.08	0.96	1.02
O−Al bond	1.86	1.85	1.98	1.73
O−Si bond	1.69	1.68	1.69	−
C(1)−C(2)−N angle	179.4	179.5	179.5	178.4
C(2)−N−H angle	165.4	170.8	153.0	161.3
N−H−O angle	172.4	175.8	173.0	
Si−O−Al angle	128.8	126.5	131.3	
Al−O−H angle	109.0	113.7		
Si−O−H angle	112.7	114.5		
Angle between vector C(2)−N in P1 and that in P2	103.7			

[a] Bond lengths are in angstroms and bond angles in degrees.

TABLE 2: Structural Parameters of Hydrogen Bonded Acetonitrile in Position 1 of CHA at Various Simulation Temperatures

property[a]	static structure	77 K	300 K	450 K
C(1)−C(2) bond	1.45	1.443 (0.011)	1.447 (0.030)	1.451 (0.040)
C(2)−N−H angle	1.16	1.161 (0.03)	1.162 (0.010)	1.165 (0.017)
N−H bond	1.56	1.552 (0.071)	1.592 (0.146)	1.688 (0.211)
H−O bond	1.06	1.059 (0.016)	1.063 (0.047)	1.052 (0.055)
O−Al bond	1.86	1.851 (0.018)	1.858 (0.046)	1.870 (0.055)
O−Si bond	1.69	1.690 (0.015)	1.698 (0.039)	1.705 (0.045)
C(1)−C(2)−N angle	179.4	177.0 (1.4)	172.6 (3.3)	171.2 (3.9)
C(2)−N−H angle	165.4	161.6 (7.6)	159.3 (10.2)	149.2 (13.8)
N−H−O angle	172.4	172.6 (3.1)	167.8 (5.8)	164.4 (8.4)
Si−O−Al angle	128.8	131.3 (2.7)	131.2 (5.1)	130.3 (6.1)
Al−O−H angle	109.0	111.9 (2.9)	115.5 (5.2)	110.4 (6.7)
Si−O−H angle	112.7	113.0 (2.7)	112.6 (5.1)	111.9 (5.4)

[a] Bond lengths are in angstroms and bond angles n degrees. Numbers in parentheses are standard deviations.

TABLE 3: Orientation of Position 1 H−Bonded Acetonitrile and Fixed Laboratory Frame with Respect to Eight-Membered Ring in CHA Unit Cell[a]

angle (degrees)	static structure	77 K	300 K	450 K
between C(2)−N bond vector and average ring plane	P1: 58.5 P2: −44.3	59.8 (10.1)	55.3 (14.8)	52.5 (18.6)
H−O bond vector and average ring plane	P1: 36.3 P2: −31.6	49.7 (6.4)	45.2 (14.2)	44.7 (16.1)
C(2)−N bond vector and H−O vector	P1: 22.4 P2: 13.7	24.5 (9.7)	24.6 (12.5)	35.2 (17.5)
x-axis of lab. frame and average ring plane		−24.2	−31.2	−30.9
y-axis of lab. frame and average ring plane		−6.2	−3.7	−4.0

[a] Plane of eight-membered CHA ring defined as passing through Al Atom and two next Si atoms. P1 designates position 1, P2 designates position 2. Columns 3−5, standard deviations are in parentheses.

structure. Whereas the structure of the adsorbed acetonitrile molecule remains essentially that of a nearly rigid symmetric top at all simulation temperatures, the parameters relating the molecule to the CHA framework exhibit large fluctuations. Further, the molecular motions relating to different degrees of freedom during the 4.5 ps trajectory do not appear to be correlated. This is illustrated in Table 3 where it can be seen that, for the static structure, the angle between the C(2)−N bond vector and H−O vector is simply the difference between the bond angle these vectors make with the plane of the eight-membered ring of CHA. This, however, is not the case for the simulations at all three temperatures. Here the average angle between the H−O vector and the ring plane, as well as the standard deviations, approaches that of the C(2)−N vector, even though the difference in the *average* angle of these vectors with respect to the ring does approximate the angle between these two vectors. Another important observation is the unusually large floppyness of the framework in the vicinity of the acid site. This undoubtedly gives rise to the possibility of a reorientational transition between position 1 and position 2 in the CHA framework.

To compare the simulations with molecular motions of the adsorbed molecule derived from NMR experiments (section 4), it is important to note that the NMR line shapes depend strongly on molecular reorientations relative to a fixed laboratory frame (the applied magnetic field, Figure 2). The molecular motions obtained from the simulations at the three temperatures in the laboratory frame are illustrated using the trajectories and histograms shown in Figures3 and 4. For these figures, the average direction of the C(1)−N vector, which describes the motion of the molecular axis in *one* of the randomly oriented crystallites, defines the *z*-axis in the fixed laboratory frame. The

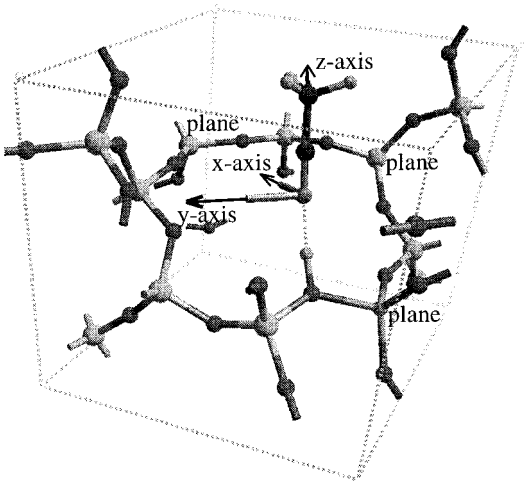

Figure 2. The *x*, *y*, and *z* axes of a laboratory frame used for the projections in Figure 3, relative to the H−CHA unit cell. The *z*-axis is defined by the average orientation of the C(1)−N vector of the adsorbed molecule.

average direction of the C(1)−N vector was computed using the last 4.5 ps (27001 time steps) of the calculation. Since the structure of the molecule in the adsorbed complex can be described as an asymmetric top at all temperatures, the *z* direction is, for all practical purposes, also described by the C(2)−N vector, whose average position relative to the eight-membered CHA ring is given in Table 3. Two axes, *x* and *y*, perpendicular to the *z*-axis were generated. The *x* and *y* axes are the minor and major axes, respectively, of an ellipse describing the motion of the C(1)−N vector of the adsorbed acetonitrile molecule at 77 K, projected onto a plane perpendicular to the *z*-axis. The relationship between these *x*, *y*, and *z* axes and the zeolite unit cell are illustrated in Figure 2, and particular values of *x* and *y* are shown in the last two rows of Table 3. The trajectories, Figure 3, show the projection onto the *x*−*y* plane of a unit vector along the C(1)−N direction for each of the time steps. The average orientation of the molecule is a unit vector perpendicular to the page starting at the origin ($x = y = 0$). Figure 4 shows histogram plots for the frequency of occurrence of *x* and *y* values, respectively, for each of the three temperatures. Clearly the potential energy surface associated with this (simulated) motion complex is far from simple harmonic.

The trajectories for the 77 K simulation seem to show a highly eccentric behavior, which is less pronounced at the higher temperatures. It is unclear whether this is a result of the finite length of the simulation or whether this eccentricity is to be expected over a long time average. Indeed, an eccentricity calculated using the standard deviations for the *x* and *y* distributions yields roughly the same value for the 450 K simulations as does such a calculation for the 77 K simulation, though the major and minor axes for the two are rotated by 90°. For the time being, we assume that the apparent eccentricity is simply a result of the limited statistics and that, to a good approximation, all of these trajectories can be regarded as the result of a simple tilting motion with axial symmetry of the molecular axis of adsorbed acetonitrile with respect to its average in the laboratory frame.

We also point out that the standard deviation for angles other than the overall tilt of the molecule (for example, the C(1)−C(2)−N angle) are all relatively small compared to the overall motion of the molecule, so it is a good approximation to treat the molecule as rigid and that the principle motion is a libration about the hydrogen bond. One assumption that will be used later when developing the NMR line shape model is that the rotation of the CH_3 group is uncorrelated with the overall tilting motion of the molecule. No obvious correlation could be seen when visualizing the trajectory nor in the data in Tables 2 and 3.

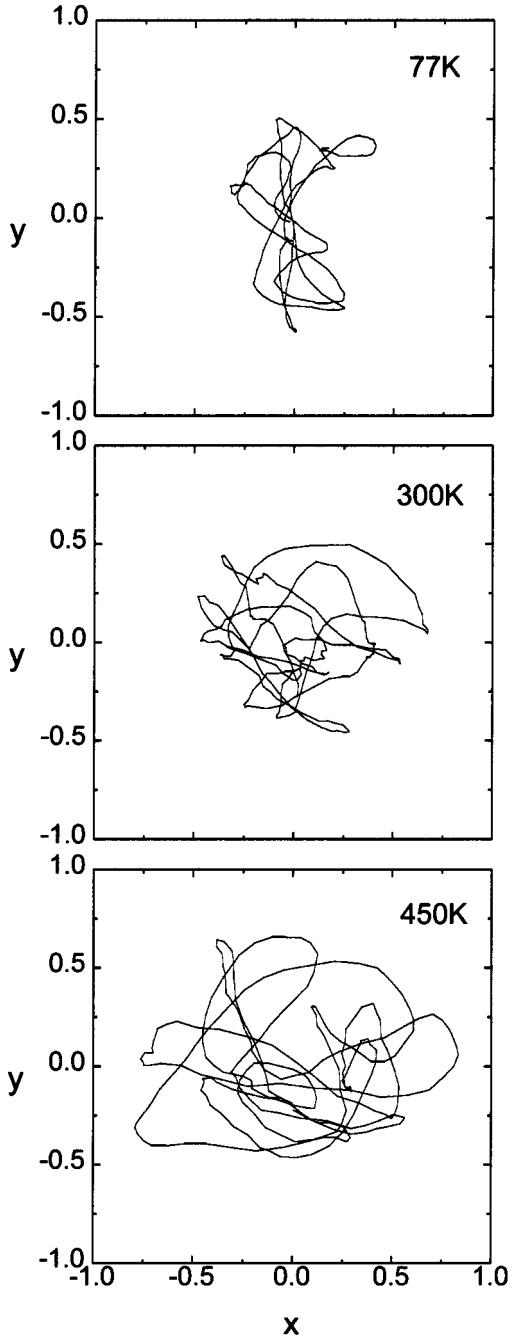

Figure 3. Projections of a unit vector along the C(1)−N direction onto the *x*−*y* plane for the three simulation temperatures. Here, the *z*-axis points along the average orientation of C(1)−N and every 100th step was used for plotting purposes.

2.4. Reaction Coordinate and Barrier for the Transitions between Position 1 and Position 2. The NMR spectra (section 4, and in particular subsection 4.4 described below) at temperatures above 360 K showed evidence of a decreased anisotropy in the powder patterns (see section 4, in particular section 4.4) which could be ascribed to large-amplitude reorientations of the adsorbed molecule in the zeolite framework, in the millisecond or sub-millisecond time scale. One possible explanation for this observation is the hopping of the hydrogen-bonded

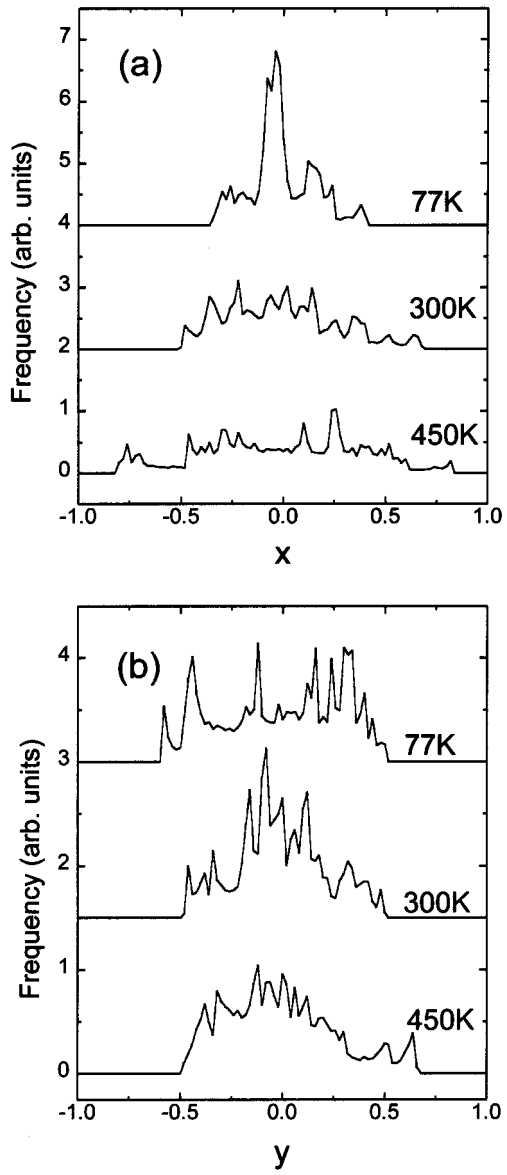

Figure 4. Histograms showing the frequency of occurrence of (a) *x* and (b) *y* values during time of evolution of the three simulations. The 77 and 300 K data have been offset from zero to aid visibility.

acetonitrile across the eight-membered ring of CHA (see Figure 1) to a stable H-bonded position on the opposite side of the ring. In section 2.3 above, we have indeed shown an additional stable position in CHA labeled position 2. The question then is how accessible is position 2 from position 1. Can in fact the acetonitrile molecule hop across the eight-membered ring without desorbing?

To address this question, we have performed a series of constrained optimizations, to determine the barrier for the motion from position 1 to position 2 and vice-versa. The constraint we have chosen is the out-of-plane angle between the O−N vector (see Figure 1) and the plane containing the protonated oxygen atom labeled in Figure 1 and the two next nearest neighbor oxygen atoms in the eight-membered ring. The results of these constrained optimizations are presented in Figure 5. The reference energy is that of the optimized structure with the H-bonded acetonitrile molecule at Position 2.

Whether starting from position 1 (squares) or position 2 (circles), both curves are continually increasing in energy, indicating that the chosen reaction coordinate does not explicitly

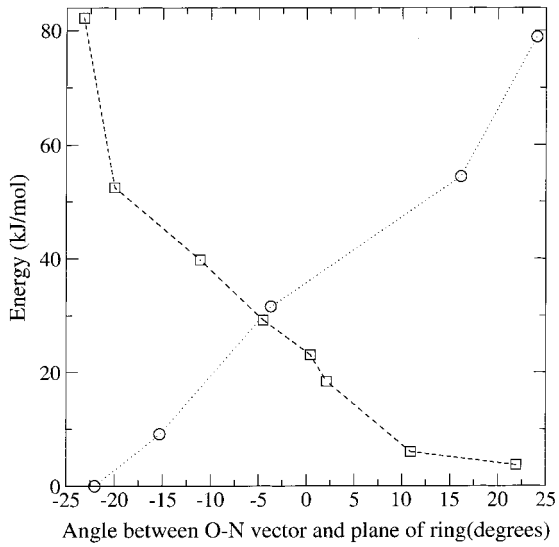

Figure 5. Energy profile for the motion of acetonitrile from Position 1 to Position 2 (squarest dashed line) and from Position 2 to Position 1 (circles and dotted line). The reference energy is that of the optimized structure with acetonitrile at position 2. For positions 1 and 2, the optimized angles between the O−N vector and the plane of the ring are 21.9 and −22.0 degrees, respectively.

link position 1 and position 2. The potential energy surface is decidedly highly corrugated, and therefore, no simple reaction coordinate can be expected to link the two positions. Nevertheless the results provide some useful insights. During the constrained optimizations, we observed that for the methyl group in the acetonitrile to be able to clear the ring completely and move to the opposite side, the angle between the O−N vector and the plane of the ring had to be changed to above 20 or below −20 degrees. The optimized values for positions 1 and 2 were 21.9 and −22.0, respectively. However increasing the angle beyond 20 or −20 degrees, after the methyl group has cleared the ring, is not accompanied by the expected decrease in energy. Instead a small change in angle produces a large increase in energy, indicating that the present method for sampling the transition pathway is inappropriate. To test this, either constrained dynamics would have to be performed,[48] or another method for sampling transition pathways that does not rely on a simply defined reaction coordinate be used.[49] While the present results do not identify the transition state, they do provide an estimate for the energy barrier associated with the transition. This can be made from the data in Figure 5 by assuming that after the methyl group has cleared the ring, then relaxation would allow the acetonitrile molecule to find its optimum position without needing to surpass any further barrier. Since the methyl group cleared the ring at about 20 or −20 degrees (depending on the direction of hopping), we expect the barrier to lie in the range 60−80 kJ/mol.

3. Experimental Section

3.1 Brønsted Site Density. The simultaneous temperature programmed desorption (TPD) and thermogravimetric analysis (TGA) measurements to determine the acid site density were carried out with 10 to 20 mg of sample, spread over the sample pan of a Cahn 2000 microbalance.[50] After saturating the sample with the vapor of the adsorbate of interest, the sample was evacuated to below 10^{-6} Torr for 1 h before beginning the 20-K/min, linear temperature ramp. Desorption products were monitored using a quadrupole mass spectrometer in the same vacuum chamber.

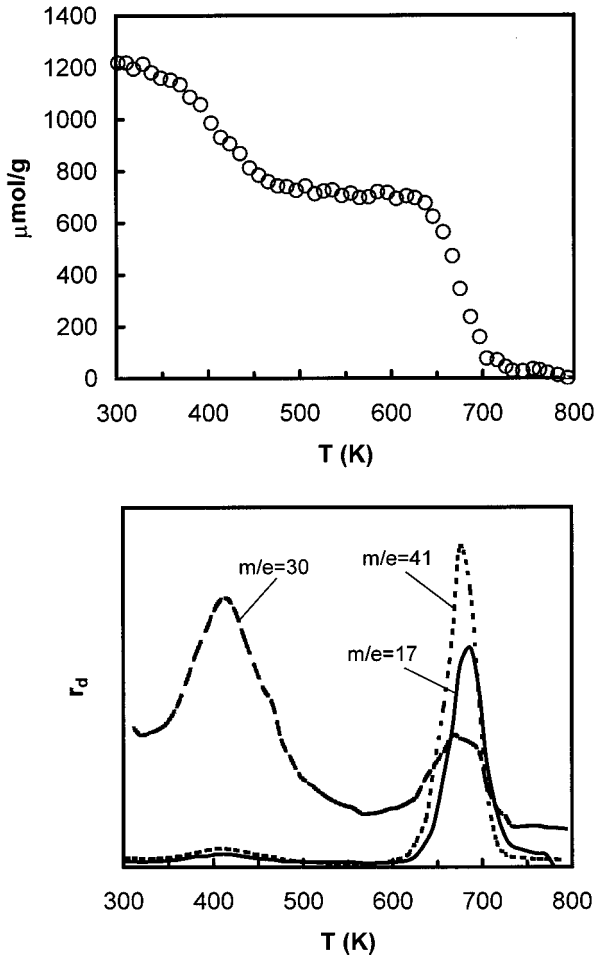

Figure 6. TPD−TGA curves for *n*-propylamine in H−CHA. The desorption products are *n*-propylamine ($m/e = 30$), propene ($m/e = 41$) and ammonia ($m/e = 17$). r_d is the desorption rate proportional to the partial pressure.

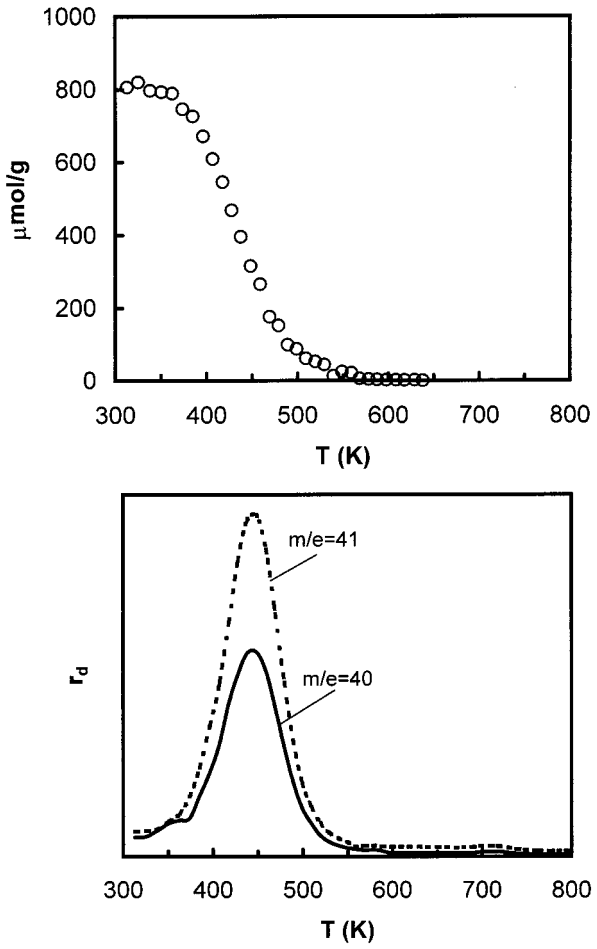

Figure 7. TPD−TGA curves for acetonitrile ($m/e = 40$ and 41) in H−CHA.

The CHA sample used in this study was obtained from S. Zones in the ammonium form and was reported to have a SiO_2/Al_2O_3 ratio of 40. The sample was simply heated in a vacuum to 750 K to form the acidic, hydrogen form. TPD-TGA measurements with *n*-propylamine on the H−CHA, shown in Figure 6, indicated that the Brønsted-site density of the sample was ∼700 μmol/g, which is somewhat less than the bulk Al content of 830 μmol/g. The determination of Brønsted-site density using *n*-propylamine on small-pore zeolites, for which the details of the adsorption procedure are described in more detail elsewhere,[51,52] rely on the fact that *n*-propylamine molecules that are protonated by the Brønsted-acid sites decompose to propene and ammonia in a narrow temperature region, between 625 and 700 K, via a reaction similar to the Hoffman elimination reaction.[53] All of the molecules desorbing below 500 K leave the sample unreacted. Since the presence of nonframework Al within the structure tends to result in the desorption of unreacted amine molecules above 500 K,[54] the well-defined plateau region in the TGA of Figure 6 implies that this material is relatively free of nonframework material.

The TPD−TGA results for acetonitrile in H−CHA, carried out in a vacuum of 10^{-6} Torr and shown in Figure 7, are very similar to those observed on H-MFI in an earlier study.[55] Following a saturation exposure and brief evacuation, the acetonitrile loading was ∼800 μmol/g, only slightly above the Brønsted site density. Most of this acetonitrile desorbed in a single peak centered at ∼400 K. This result is important for two reasons. First, it provides strong evidence for a 1:1 adsorption complex between acetonitrile and the Brønsted sites. Second, it demonstrates that there will be rapid motion of the adsorbed acetonitrile above 400 K. Caution must be used in the determination of energetics from these results since diffusion and readsorption typically raise the desorption peak temperature for TPD from a porous material, even when the experiments are carried out in a vacuum.[56] However, if readsorption and diffusion were negligible, a desorption peak temperature of 400 K would correspond to heats of adsorption of ∼120 kJ/mol for a normal, first-order process.[57] This provides an approximate upper limit for the adsorption energetics.

3.2. Calorimetric Studies. The microcalorimetry measurements for acetonitrile used equipment and procedures that have been described elsewhere.[58] The home-built, Calvet-type microcalorimeter allowed the use of relatively large samples (∼1 g) spread into a very thin bed (∼1 mm thick) for rapid adsorption and rapid heat transfer to the thermopiles. Adsorption was performed at 400 K to enhance adsorbate mobility to the acid sites.[59]

The differential heats of adsorption for acetonitrile in the H−CHA, measured calorimetrically at 400 K, are shown in Figure 8. The data show relatively constant differential heats of ∼100 kJ/mol to above 500 μmol/g. At higher loadings, the differential heats show a gradual decline to ∼80 kJ/mol, and it is likely that even lower heats would have been observed if higher loadings had been examined. Because this instrument was not designed to measure heats of adsorption when gas-phase species are in equilibrium with the adsorbate, measured

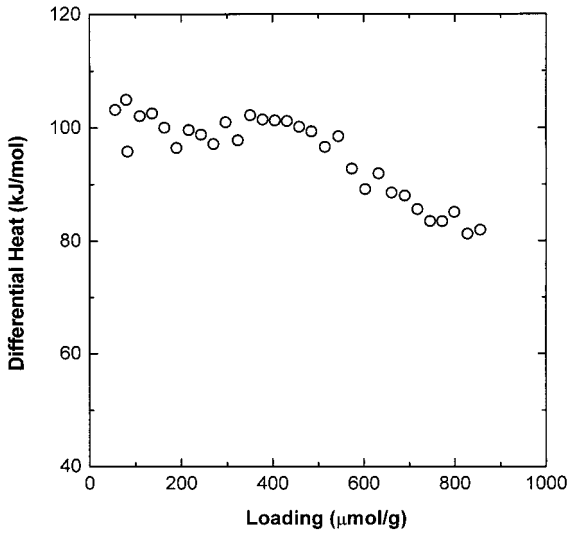

Figure 8. Differential heats of adsorption for acetonitrile in H−CHA. The measurements were performed at 400 K.

heats at higher loadings are unreliable and thus were not pursued. On the basis of results in MFI, one would expect physisorbed molecules to have a heat of adsorption of approximately 60 kJ/mol.[55,60]

We interpret the results at the low loadings as indicating that the bonding interaction is essentially the same for acetonitrile with all of the Brønsted-acid sites. The scatter in these data reflects the precision measure of the technique rather than any indication of a measurable distribution of sites. The absence of a significant vapor phase at such low loadings combined with the extremely slow site-to-site diffusion of acetonitrile adsorbed at the acid sites in the framework at 400 K[59,61] would not permit the observation of site distribution calorimetrically under our experimental conditions, even if they did exist. The fact that the differential heats begin to fall at a coverage slightly below the Brønsted-site density that had been measured in TPD-TGA is probably also not significant.

3.3. Multinuclear NMR Studies. Both the protonated and deuterated forms of CHA were employed in these studies. To obtain the deuterated form of the sample, H−CHA was repeatedly exposed to D_2O vapor and evacuated, after which the sample was gradually heated to 750 K in vacuo until the pressure fell below 10^{-6} Torr. Using NMR as the analytical tool, it was found that the proton background of the deuterated samples were always less than 3% of the total signal when CH_3CN was adsorbed.

For the NMR measurements, approximately 150 mg of CHA was degassed and weighed at 700 K in a Cahn microbalance at 10^{-6} Torr. As in our earlier MFI studies,[22] the samples were then transferred into specially designed glass sample tubes which were then attached to a vacuum manifold and again degassed at 700 K and 10^{-6} Torr.[62] The degassed samples were exposed to controlled amounts acetonitrile vapor for the proton studies, deuterated acetonitrile for the deuterium studies, and the labeled compound (C-1, 99% ^{13}C enriched, Cambridge Isotope Labs. Inc.) for the ^{13}C NMR measurements using a calibrated volume that allowed the adsorbate coverage to be known to within 2%. To avoid bed effects upon adsorption, the zeolite was spread along a length of a long, evacuated, 1/2 in. diameter tube during exposure to the gaseous adsorbate[62,63] and then poured into a smaller tube without exposure to air. NMR spin counting measurements were used as a check of the volumetric zeolite loadings.

The ^{13}C, ^{1}H, and ^{2}H NMR spectra were obtained at a magnetic field of 3.5 T (37.84 MHz for ^{13}C, 150 MHz for ^{1}H, and 23.11 MHz for ^{2}H resonance). ^{13}C and ^{2}H NMR measurements were also performed at 8.4 T (90.7 and 55.4 MHz for ^{13}C and ^{2}H, respectively) to explore the effect of frequency. All measurements were performed using a previously described home-built spectrometer and probe,[22,64] in conjunction with a Libra pulse programmer and software provided by Tecmag.[65]

For the ^{13}C powder patterns, the line shapes and frequencies were determined from the observation of proton-decoupled, 90°-τ-180°-τ-acquire, Hahn-echo pulse sequences in quadrature and with time delay, τ, varying from 30 to 50 μs. Unfortunately, for the low adsorbate loadings used in these experiments, cross polarization did not lead to significant signal enhancement. The pulse cycle for both the methyl proton and deuterium line shapes was the quadrupolar echo sequence, $(90°)_0$-τ_1-$(90°)_{90°}$-τ_1-acquire. In the case of the methyl protons at low temperatures, the delay time, τ_1, was set at 74 μs in order to obtain a line shape characteristic of a free-induction decay. As demonstrated earlier in the study of matrix-isolated acetonitrile,[66] the three methyl protons behave as a quasi-quadrupolar nucleus of spin 3/2; but, due to dipolar coherences, the line shapes are dependent on the quadrupolar echo delay time.[5,67,68] As will be seen from the data presented below, small changes in the dipolar couplings occur with increasing temperature. However, measurements with values of τ_1 corresponding to the averaged dipolar couplings at any given temperature showed little if any change in the spectra from those presented here. For the ^{2}H NMR spectra of CD_3CN, the delay times were 60 μs and the line shapes did not show any significant changes on varying the delays in the range from 30 to 90 μs.

For all spectra, the repetition rate on signal averaging was greater than twice the spin−lattice relaxation time ($2T_1$) to avoid significant saturation effects. Since the quantity of adsorbed molecules in most samples was of the order of 65 micromoles, the number of scans required to obtain reasonable signal-to-noise was large. For the ^{1}H NMR spectra, several hundred scans were required at 78 K and a thousand or so in the vicinity of room temperature. For the ^{2}H NMR spectra, the number of required scans was almost factor of 10 higher over this temperature range, while for the ^{13}C NMR spectra the necessary scans were approximately five greater in order to obtain a reasonable signal-to-noise ratio.

3.4. Experimental NMR Powder Patterns. Three CHA samples from a common batch of material were used for studying the temperature dependence of the powder line shapes of the 1:1 acetonitrile adsorption complex. In each case, however, the acetonitrile loading based on the TPD-measured Brønsted site density was 0.70 ± 0.05 molecules per acid site.

The ^{1}H-dipolar, ^{13}C-chemical-shielding, and ^{2}H-quadrupolar powder patterns for the stoichiometric aceronitrile adsorption complex at a magnetic field of 3.5 T are shown in Figures 9, 10, 11, and 13, at temperatures ranging from 78 to 410 K. Figure 9 shows the entire ^{1}H NMR line shapes for CH_3CN in the deuterated CHA, while the spectra in Figure 10 contain only 20% of the central line so as to display more clearly the temperature-sensitive dipolar powder patterns. As in the case of the H-MFI adsorption complex,[22] the powder line shape at 78 K is characteristic of a spatially isolated methyl group, freely rotating about a fixed axis (C_3 symmetry axis of the molecule) in a plane perpendicular to this axis.[66,67] The dipolar splitting, measured from the separation of the sharp features in the spectrum, is 29.9 kHz. This is only 0.03 kHz less than a "rigid-lattice" value obtained for the freely rotating or tunneling methyl

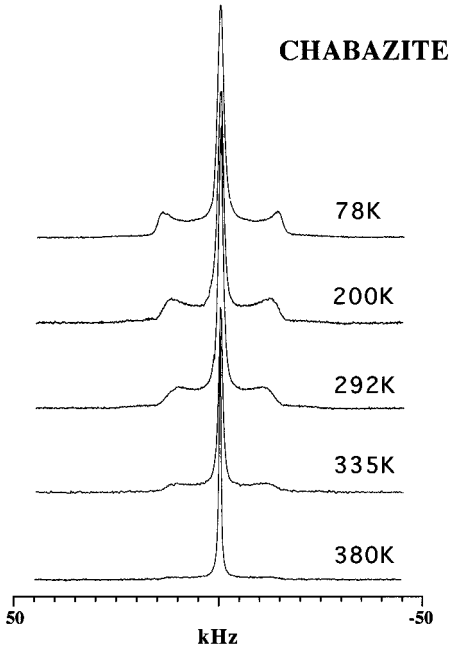

Figure 9. Methyl proton spectra of 1:1 acetonitrile adsorption complex in D−CHA as a function of temperature (0.7 molecules per Brønsted site).

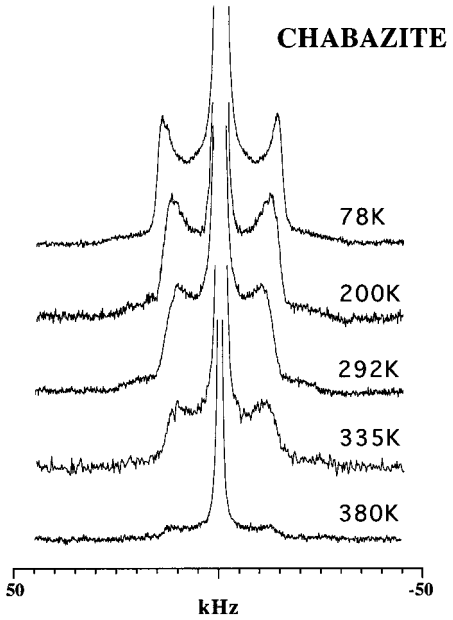

Figure 10. The data of Figure 8 scaled to show the dipolar portion of the proton NMR spectra.

group of matrix isolated acetonitrile in krypton at 4.9 K.[66,67] With increasing temperature between 78 and 360 K, this splitting decreases monotonically while the sharp discontinuities of the powder pattern display some broadening. At higher temperatures, however, some significant changes begin to occur. This is illustrated in the spectrum at 380 K, which shows a marked decrease in the intensity of the dipolar features as well as a narrowing of the central line at the resonance frequency. At temperatures above 400 K only a narrow Lorentzian central feature is observed. This type of behavior is characteristic of the line shape changes for all three nuclei of the acetonitrile molecule presented here. In all cases at low temperatures this type of behavior can be accounted for in terms of the libration amplitudes of the localized molecular axis, and larger angle reorientations due to site exchange at the higher temperatures.

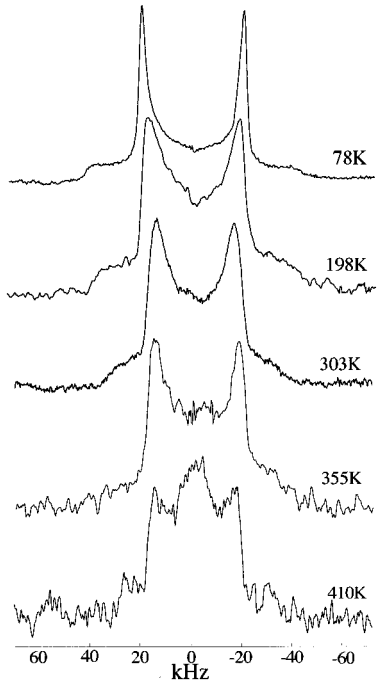

Figure 11. Methyl deuterium quadrupole powder patterns of the 1:1 CD_3CN stoichiometric adsorption complex in H−CHA as a function of temperature. (0.7 molecules per Brønsted site).

The latter is consistent with the peak desorption temperature observed from TPD of acetonitrile in vacuo described in section 3.1.

The temperature dependence of the methyl-group deuterium quadrupolar powder patterns for CD_3CN adsorbed in H−CHA are shown in Figure 11. At 78 K, the sharp features of the spectrum correspond to that of an axially symmetric powder pattern with an average quadrupolar-coupling constant of 39 kHz. This, like the methyl-proton pattern discussed above, is typical of a CD_3 group reorienting rapidly about its fixed, C_3 symmetry axis, with a splitting close to that of the "rigid lattice". For the neat solid at 78 K, where the barriers to molecular reorientation are considerably higher, we have measured a quadrupolar splitting of 40 kHz. In Figure 12, the changes in the proton dipolar and deuterium quadrupolar splittings with temperature are compared, assuming that one observes a splitting corresponding to 99% of that exhibited by the "rigid lattice" for both cases at 78 K. Within experimental error, the trends appear to be the same for both nuclei in the temperature range 78 to 360 K It is also interesting to note that above 250 K the splittings in both cases seem to approach a limiting value, suggesting the presence of a constraint, imposed on the anisotropic motion prior to desorption, by the size of the framework cavity. Above 360 K, however, where large amplitude reorientations and desorption become important, both ^1H and ^2H powder patterns indicate a change in the character of the molecular motion. At 410 K, a prominent central feature begins to appear in the quadrupolar spectrum, suggesting the possibility of a superposition of two types of spectra. One type corresponds to molecules that remain bound to the acid site on the time scale of the NMR measurement (milliseconds), and a second type corresponds to molecules undergoing more nearly isotropic motion in the zeolite cavity. In fact, at even higher temperatures, the ^2H line shapes reduce to motionally narrowed Lorentzians.

The proton-decoupled, axially symmetric, ^{13}C NMR spectra as a function of temperature are shown in Figure 13. At 78 K,

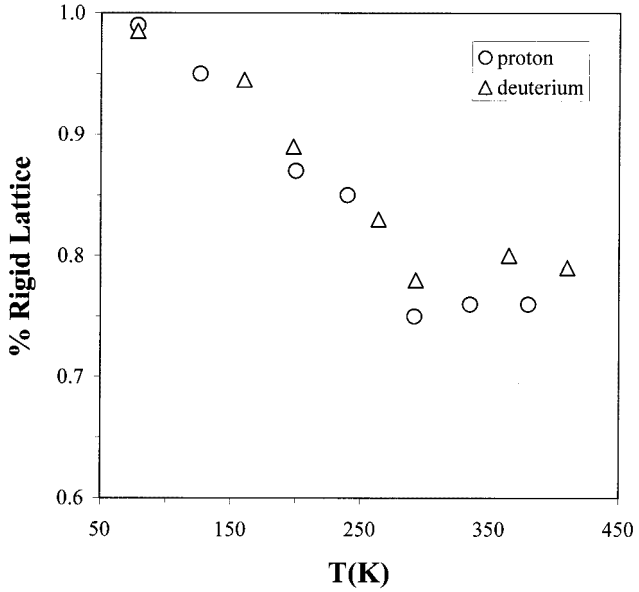

Figure 12. dipolar (○) and quadrupolar (△) splittings of methyl proton and deuterium powder patterns, respectively, as a function of temperature.

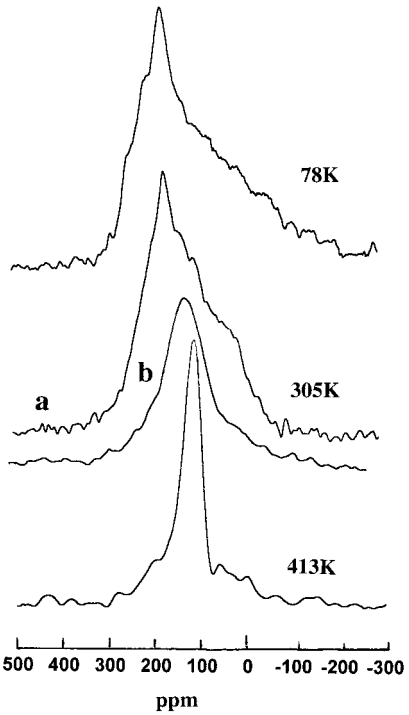

Figure 13. Proton decoupled nitrile ^{13}C-chemical shielding powder patterns of 1:1 CH_3CN stoichiometric adsorption complex in H−CHA as a function of temperature (0.7 molecules per Brønsted site at 78, 305 (a), and 413 K. The second spectrum at 305 K (b) corresponds to 1.2 molecules per acid site. The ppm scale is relative to liquid TMS at 295 K).

a broadened "rigid-lattice" chemical-shielding powder pattern is observed that includes features due to the ^{13}C-^{14}N dipole interactions.[5] As in the case of the MFI studies,[22] the spectral features due to this tensor permit the determination of the orientation of the principal components of the ^{13}C chemical shielding relative to the ^{14}N electric-field gradients. Given the large uncertainty in the frequency of these features, one can only conclude that the spectral parameters of both the CH_3CN−H−CHA and CH_3CN−H MFI adsorption complexes are nearly the same.[5] Between 78 and 305 K, the changes in the shape of the powder patterns are minimal, except for a broadening and decrease of the anisotropy that can also be attributed to reorientations of the molecular axis. The disappearance of the structure due to the $^{13}C-^{14}N$ dipole coupling, is likely due to the fast T_1 relaxation of ^{14}N at the higher temperatures. Above 360 K, one begins to observe considerable motional narrowing, evidenced by the fact that the line shape is unaffected by proton decoupling; becoming a narrow Lorentzian at 413 K with fwhm of about 1 kHz, centered about an isotropic chemical shift of approximately 115 ppm (relative to liquid TMS at room temperature), a value close to that observed for the liquid phase.[68] Unlike the case of the adsorbed CH_3CN in H-MFI, there are no reversible (or irreversible) changes in the isotropic chemical shift on temperature cycling between 400 and 500K.[68,69]

Some general statements can be made in the comparison of the acetonitrile ^1H, ^2H and ^{13}C NMR line shapes in the two zeolites, MFI and CHA, investigated to date. First, at the lowest temperatures, the anisotropic line shapes are nearly identical in both cases. Second, the effect of temperature on the motional narrowing of these anisotropic line shapes, although not identical, is somewhat similar in that these effects occur over a similar temperature range but at temperatures approximately 50 degrees higher in CHA than in MFI. This is not surprising given that the confinement of the acetonitrile near the smaller eight-membered framework rings of CHA gives rise to a larger barrier to molecular reorientations. However, what differs considerably is the behavior of the adsorption complex at greater loadings. Unlike MFI, higher loadings do not lead to the catastrophic motional narrowing of the ^{13}C line shapes in CHA when the loading exceeds one molecule per acid site (Figure 13, see 305 K (b) spectrum, 1.2 molecules per acid site).[5,70] This again may be attributable to the larger barriers to molecular reorientations in H−CHA.

4. NMR Line Shape Modeling: Comparison of Theory with Experiment

4.1. Analytical Model. An NMR line shape model previously developed to account for motion of the hydrogen-bonded CH_3CN molecule in H-MFI[22] adequately describes the line shape changes observed here as well. This model treats a spatially and magnetically isolated acetonitrile molecule as a rigid linear system with a rapidly rotating CH_3 or CD_3 group in a plane perpendicular to the C_3 symmetry axis of the adsorbed molecule. The orientation of the molecular axis is defined by the C−C−N bond of the adsorption complex. In this model, the NMR line shape changes with temperature are affected by the libration of the molecular axis within the zeolite framework. The frequencies of these motions are assumed to be very large compared to the NMR frequency, consistent with the results of the molecular dynamics simulations. Further, the rotational motion of the CH_3 or CD_3 group is assumed to be uncorrelated with the molecular libration.

Here we consider changes in the NMR powder patterns of three isotopic species of the hydrogen-bonded acetonitrile adsorption complex in CHA due to molecular motion. Within the rigid-molecule approximation, the underlying molecular motion determining the ^1H NMR spectra of CH_3CN, the ^{13}C spectra of $CH_3{}^{13}CN$, and the ^2H spectra of CD_3CN must be the same for all three cases. The NMR shifts for ^1H are principally due to the H−H nuclear dipole interactions. As long as the three ^1H nuclei remain equivalent, they give rise to a pseudo-quadrupolar spectrum, which is axial along the molecular axis, arising from total nuclear spin 3/2, combined with single-line

spectra from the total spin 1/2 case.[66] In the case of ^{13}C NMR spectra, the shifts are due to the combination of an axial chemical shift ($\nu_| = 104$ ppm relative to the isotropic shift of liquid TMS at 295 K, or 4 kHz at 3.5 T) and the $^{13}C-^{14}N$ nuclear dipole interaction (0 and ± 1.4 kHz). Both of those interactions are axial along the molecular axis.[71] The shifts in the ^2H NMR spectra are predominately due to the time-average electric quadrupole interaction in the presence of a rapidly rotating CD_3 group. Due to the rapid rotation, the electric quadrupole interaction can be described by an average Hamiltonian that is axial along the molecular axis.[72]

4.2. Librational Amplitudes from NMR Line Shapes. In the reference frame of a stationary molecule, where the *z*-axis is along the molecular axis, the spectra for all three nuclei in the absence of motion can be written as the result of a sum over all orientations of the magnetic field of the signal, *S*, which is (or would be) observed for each orientation

$$S(\theta,\vartheta) = \sum_{k=1}^{n} \delta(\omega - \omega_0 - \omega_k)$$

$$\omega_k = \omega_{k0}(1 - 3\cos^2\theta)$$

Here, $\delta(\omega)$ is the dirac delta function, θ and φ are the usual polar coordinates describing the orientation of the applied magnetic field within the molecular frame, and ω_0 is the center frequency, which includes isotropic shifts. We are not concerned with isotropic shifts in the model. Values of *n*, *k*, and ω_k for the three cases can be found in ref 22.

To calculate the line shapes in the presence of rapid molecular reorientation, we take the z-axis to be along the time-averaged orientation of the molecular axis. The relationship of this laboratory frame axis to the zeolite structure is described in section 2.3 and shown in Figure 2. We use a classical model where the instantaneous frequency is given by $\omega_{k0}(1 - 3\cos^2\theta')$, where θ' is the angle between the applied magnetic field and the instantaneous orientation of the molecular axis. The motion is assumed to be always very rapid compared with ω_k, so the observed frequency, $\bar{\omega}_k$,will then be the time average of the instantaneous frequencies. The instantaneous orientation of the molecule is described using polar angles (α, ξ) corresponding to a rotation about the *y*-axis by an angle α followed by a rotation about the z-axis by an angle ξ. α is the angle between the instantaneous orientation of the molecule and its average orientation. Then, $p(\alpha, \xi)$ is the probability (per unit solid angle) that the molecule will be found at (α, ξ). An average over time is then accomplished by writing θ' in terms of (α, ξ) and averaging over all angles.

Further computation requires knowledge of $p(\alpha, \xi)$. In a previous paper,[22] several different distributions were considered. Examination of the spectra shows that except at the very highest temperatures shown, the spectra have the characteristic shape of a powder pattern in the presence of an axial interaction. As the temperature changes, only the overall frequency scale of the interaction changes. This suggests the "2-d" model as most appropriate.[73] This is consistent with the trajectories obtained from the simulations shown in Figure 3, except possibly at 77 K where some anisotropy is seen at least for the limited time scale of the simulations. The 2-D model assumes all values of the angle ξ occur with equal probability. With such a model, the line shape will look identical to the line shape in the absence of motion, except with an overall scale factor for the frequency scale. Examination of the NMR spectra, especially the ^2H spectra, shows that except for a small broadening of the sharp features this is at least approximately what is happening below 360 K. This broadening can be attributed to a distribution of acid sites, energetically similar but somewhat different dynamically. Evidence for this lies not only in the observation of two nearly equivalent positions of the adsorbed acetonitrile in the unit cell, but also in the existence of 4 possible symmetry-inequivalent acid-site configurations.[16] The simplest 2-D distribution assumes a square distribution for which all orientations with values of the angle α from 0 up to a maximum value of α_0 occur with equal probability, and the probability is zero for $\alpha > \alpha_0$. With that model,

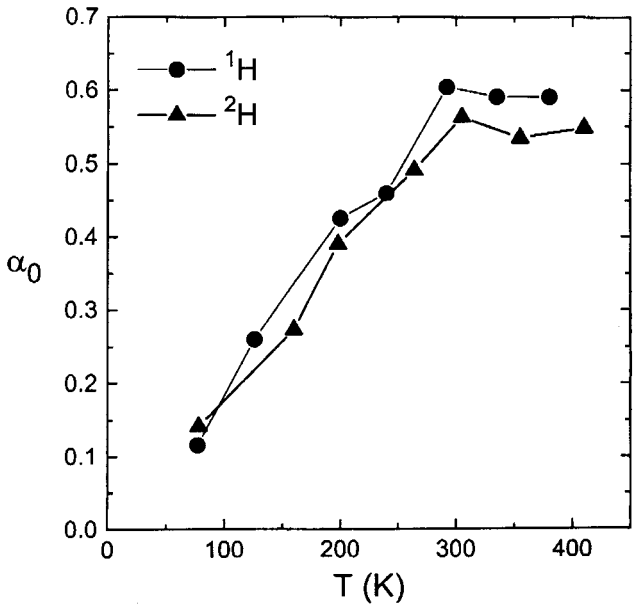

Figure 14. Values of the overall amplitudes of motion, α_o, (in radians) for a square distribution derived from the dipolar and quadrupolar measured splittings (Figure 12), as a function of temperature.

$$\bar{\omega}_k = \frac{\omega_{k0}}{2}[\cos\alpha_0(1 + \cos\alpha_0)](1 - 3\cos^2\theta)$$

Hence, the angle α_0, which describes the overall amplitude of the motion, can be deduced, for example, by looking at the splitting between the two peaks of the ^2H spectra or the corresponding two peaks of the ^1H spectra (Figure 12) and comparing to the equation above. The results for the square distribution, are quite convenient and have the appropriate limiting behavior. Values derived using this model are shown in Figure 14.

4.3. Comparison of Theory with Experiment. The square distribution is somewhat crude, to be sure. For this square distribution one expects values of $\cos(\alpha)$ between $\cos(\alpha_0)$ and 1 to occur with equal probability. Figure 15 illustrates the frequency of occurrence of $\cos(\alpha)$ observed for the molecular dynamics simulations. These curves suggest that a half-Gaussian or Planck distribution would allow a more accurate comparison with the simulations. To make a better comparison with the simulations, we use the marginal probability distribution for $\cos(\alpha)$ given by

$$p(\cos\alpha) = \sqrt{\frac{2}{\pi\sigma^2}}\exp\left(\frac{-(1 - \cos\alpha)^2}{2\sigma^2}\right)$$

which is valid only for $\sigma \ll 1$. For that distribution we obtain

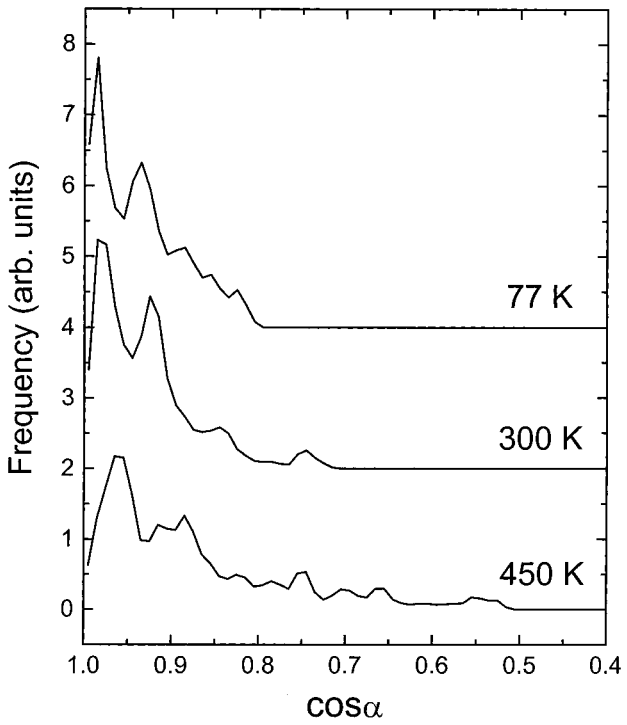

Figure 15. Histograms showing frequency of occurrence for values of cos(α) as obtained from the molecular dynamics simulations for the three temperatures. The data for 77 and 300 K have been offset from zero for clarity.

$$\bar{\omega}_k = \omega_{k0}\left(1 - \frac{3\sqrt{2}}{\pi}\sigma + \frac{3}{2}\sigma^2\right)(1 - \cos^2\theta)$$

In comparing theory with experiment, the choice of "rigid lattice" values for the peak-to-peak dipolar and quadrupolar splitting is important. Using the "rigid-lattice" peak-to-peak proton dipolar splitting for the fixed-axis CH_3CN in a solid krypton matrix[66,67] and the quadrupolar splitting for solid CD_3-CN as references, the filled circles and triangles in Figure 16 show the values of σ deduced from the spectra based on the half-Gaussian distribution. The ^1H and ^2H data are in reasonable agreement. Both show an approximately linear increase in σ from 100 K up to about 300 K, and at higher temperatures σ becomes temperature independent. Also shown on that figure are values of σ computed from the molecular dynamics simulation results. While the scale of the magnitude of the theoretical molecular fluctuations are in agreement with experimentally deduced values, the temperature dependence between theory and experiment is not particularly good. Similar disagreement is obtained using the square distribution.

This lack of agreement is independent of minor adjustments, including, for example, modifying the "rigid lattice" splittings. Using the proton dipolar splitting calculated from the proton−proton distance of 1.790 Å obtained for the optimized static structures (section 2.2) of the CH_3CN adsorption complex for both position 1 and position 2 increases the "rigid lattice" proton dipolar splitting by approximately 4%. Within an uncertainty of 0.0015 Å the six proton−proton separations in both positions are identical. This is smaller than the 1.81 Å separation of methyl protons in a krypton matrix[66] as well as 1.8024 Å in the gaseous molecule.[74] Since the observed proton and deuterium splittings, as a fraction of the "rigid lattice" values are nearly the same at all temperatures (Figure 12), this would imply a similar increase in the quadrupolar coupling constant of deuterium in the adsorption complex. Given that the electric field gradients in the vicinity of the deuterium nucleus in H−CHA cannot be the same as the neat solid, this is not unreasonable. The net effect of this change in the values of σ, as shown by the open circles and triangles in Figure 16 is, however, minor. There is better agreement between theory and experiment at the lowest temperature but the experimental trend of σ with temperature does not match the predictions of the simulations. It is important to note that the observation that the NMR spectra simply do not change above about 300 K is model-independent and that cannot be accounted for in the simulations.

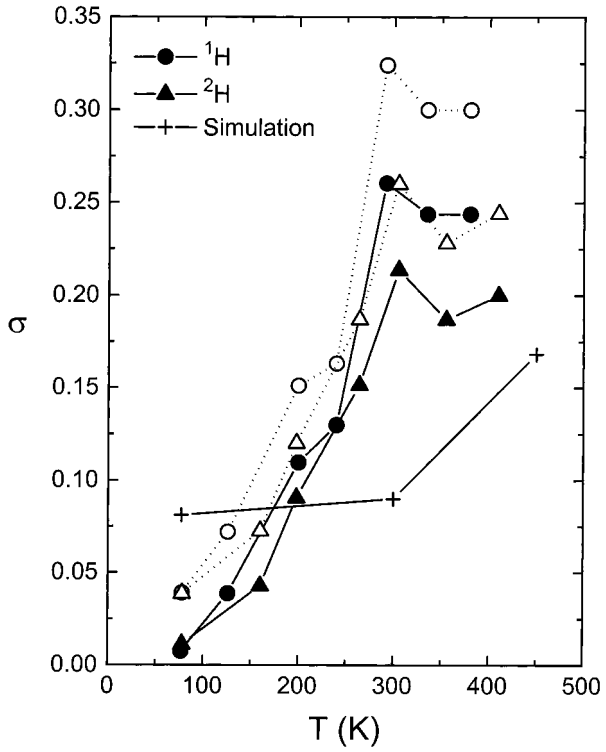

Figure 16. Values of σ derived from measured peak-to-peak splittings from deuterium and proton NMR data and using the half-Gaussian distribution for the frequency of occurrence of values of cos(α) as described in text. Values of σ derived from the simulations are standard deviations computed using distributions shown in Figure 15.

A possible explanation for this problem is that errors in the choice of the exchange-correlation functional are responsible. As noted in the discussion of the energy of chemisorption to form the acetonitrile−zeolite adsorption complex in section 2.2, the exchange-correlation functional used in the calculation does not properly treat dispersion forces. (We note that there is as yet no known exchange-correlation functional that does treat dispersion forces well.) The functional, in fact, approximates the entire range of interactions and thus will yield a potential energy hypersurface that is approximate. Errors in the repulsive regime causing it to be too soft, for example, could lead to this discrepancy. Another possible explanation is inadequate statistics in the simulations. This could be tested by running much longer trajectories using classical, fitted, potentials.

4.4. NMR Line Shapes at Elevated Temperatures. While detailed discussion of the higher temperatures (above 360 K), where large angle reorientations of the hydrogen bonded species between two stable positions in the zeolite framework as well as dissociation of the adsorption complex to form a physisorbed phase may occur, is beyond the scope of this work, some features are worth mentioning. In particular, for the ^2H spectra, a broad central peak begins to grow just above 400 K. This behavior is indicative of the onset of a more isotropic motion of the adsorbed acetonitrile molecule, which tends to motionally

average the powder pattern. This motional averaging will become observable when the rate of motion is comparable to the NMR line width. For the ^{2}H spectra, this corresponds to about 20 to 40 μs. If one assumes an Arrhenius behavior and using an "attempt frequency" of $(1\ \text{ps})^{-1}$ as typical of librational frequencies observed in the simulations, an onset of motional narrowing at 410 K corresponds to an activation energy of approximately 60 kJ/mol. This is comparable to the activation energy estimated from the simulations for motion of the molecule from position 1 to position 2 in the zeolite framework (see section 2.4). It is also comparable to the binding energy of a physisorbed molecule to the acid site. Further experiments in the high-temperature region are being pursued to study this further.

5. Conclusions

We have performed a series of Car−Parrinello simulations of the motion of adsorbed acetonitrile at a Brønsted acid site in CHA and compare the results with statistical averages of molecular motion derived from multinuclear solid state NMR experiments over a range of temperatures from 77 to 450 K, in order test of the ability of present day first-principles dynamic simulations to describe topologically sensitive interactions. From the simulations, the acetonitrile molecule is hydrogen-bonded to the acid proton at all temperatures, the essentially rigid C−C−N molecular axis lying outside the eight-membered CHA ring forming the large cavities in the zeolite structure. At 0 K the binding energy of the adsorbed molecule is in reasonable agreement with experiment when dispersion forces are taken into account.

The simulated molecular motion of the adsorption complex consists of free rotation of the methyl-group protons in a plane perpendicular to the molecular axis of the acetonitrile molecule, together with a complicated motion of this axis in the "breathing" CHA framework. The motion of the molecular axis can nevertheless be decomposed into a bending about the hydrogen bond and translation in a plane perpendicular to the hydrogen bond. From the standpoint of modeling the NMR results this complex motion, which can simply be treated as a two-dimensional libration about the hydrogen bond to describe the time dependent orientations of the adsorbed molecule, was found to be isotropic at the higher temperatures in agreement with experiment. The simulations also demonstrate that the cosine of the tilt of the molecular axis with respect to its average position, when the motion is treated as a libration, is close to a Planck distribution with the standard deviation of amplitudes within a factor of 2 of those derived from experiment. While both theory and experiment display an increase in the standard deviation of the tilt angle distribution with increasing temperature, the simulation does not properly predict the experimental trend which suggests that above 300 K, the amplitudes have reached a maximum as a result of repulsive interactions which are either not properly represented by the functionals or a result of statistical error in the length of the trajectory.

The simulations do however indicate the possibility of a penetration of the hydrogen-bonded molecule from one side of CHA eight-membered ring to the other, on a time scale much longer than was possible in the dynamic simulations. First-principles calculations found two possible positions for the adsorption of acetonitrile on a Brønsted-site associated with a particular lattice oxygen atom. These two positions had almost equal energies of adsorption and were close to mirror images across the plane of the symmetry of the eight-membered ring. The barrier for passage of the adsorbate across the ring was estimated to be between 60 and 80 kJ/mol. This is in agreement with the experimental observation of a large amplitude reorientation of the molecular axis of the adsorbed acetonitrile above 400 K which suggests transitions between two possible positions in CHA in a sub-millisecond time scale.

Finally, it is of interest to note the difference in behavior between acetonitrile adsorbed in H-MFI[22] and the acetonitrile complex in CHA. The NMR studies indicate that the molecular motions in the latter are clearly more isotropic. This is undoubtedly a result of differences in zeolite topology and location of the Brønsted site in the framework. This result is not surprising given the large difference in framework structures, but unfortunately cannot, as yet, be tested using first principles calculations due to computational limitations. The present results do, however, provide one of the first experimental tests of the limitations of, as well as insights derived from, first-principles dynamic simulations based on presently available functionals.

Acknowledgment. We especially wish to thank Dr. S. Zones for supplying us with a high-quality siliceous CHA sample, Dr. Marcel Allavena for many helpful discussions, Dr. Lichang Yang and Oferi Kresnawahjuesa for sample preparations and the TPD-TGA and calorimetric measurements. This work was supported in part by the National Science Foundation, Grant # CTS 9713023.

References and Notes

(1) Farneth, W. E.; Gorte, R. J. *Chem. Rev.* **1995**, *95*, 615.
(2) Biaglow, A. I.; Gorte, R. J.; White, D. *J. Phys. Chem.* **1993**, *97*, 7135.
(3) Šepa, J.; Lee, C.; Gorte, R. J.; White, D.; Kassab, H.; Evleth, E.; Allavena, M. *J. Phys. Chem.* **1996**, *100*, 18515.
(4) Gorte, R. J.; White, D. *Topics Catal.* **1997**, *4*, 57.
(5) Šepa, J.; Gorte, R. J.; White, D.; Kassab, E.; Allavena, M. *Chem. Phys. Lett.* **1996**, *262*, 321.
(6) Kubelkova, L.; Kotrla, J.; Florian, J. *J. Phys. Chem.* **1995**, *99*, 10285.
(7) Florian, J.; Kubelkova, L. *J. Phys. Chem.* **1994**, *98*, 8734.
(8) Pelmenschikov, A. G.; van Santen, R. A.; Jänchen, J.; Meyer, E. *J. Phys. Chem.* **1993**, *97*, 11071.
(9) Gorte, R. J.; White, D. *Microporous Mesoporous Mater.* **2000**, *35−36*, 447.
(10) Allavena, M.; Seiti, K.; Kassab, E.; Ferenczy, Gy.; Angyan, J. G. *Chem. Phys. Lett.* **1990**, *168*, 461.
(11) van Santen, R. A.; Kramer, G. S. *Chem. Rev.* **1995**, *95*, 737.
(12) (a) Brandle, M.; Sauer, J.; Dovesi, R.; Harrison, N. M. *J. Chem. Phys.* **1998**, *109*, 10379. (b) Seirka, M.; Sauer, J. *J. Chem. Phys.* **2000**, *112*, 6983.; Bentzien, J.; Muller, R. P.; Florián, J.; Warshel, A. *J. Phys. Chem. B* **1998**, *102*, 2293.
(13) Greatbank, S. P.; Hillier, I. H.; Burton, N. A.; Sherwood, P. *J. Chem. Phys.* **1996**, *105*, 3770.
(14) Nusterer, E.; Blöchl, P. E.; Schwartz, K. *Angew. Chem.* **1996**, *108*, 187.
(15) Schwartz, K.; Nusterer, E.; Blöchl, P. E. *Catal. Today* **1999**, *50*, 501.
(16) Shah, R.; Gale, J. D.; Payne, M. C. *J. Phys. Chem.* **1996**, *100*, 11688.
(17) Shah, R.; Gale, J. D.; Payne, M. C. *J. Phys. Chem. B* **1997**, *101*, 4787.
(18) Haase, F.; Sauer, J.; Hutter, J. *Chem Phys. Lett.* **1997**, *266*, 397.
(19) Stich, I.; Gale, J. D.; Terakura, K.; Payne, M. C. *J. Am. Chem. Soc.* **1999**, *121*, 3292.
(20) *Applications of Picosecond Spectroscopy to Chemistry*; Eisenthal, K. B., Ed.; Reidel Publishing Co.: Dordrecht, Boston, Lancaster, 1983.
(21) Zaborowski, E.; Zimmermann, H.; Vega, S. *J. Am. Chem. Soc.* **1998**, *120*, 8113.
(22) Suits, B. H.; Šepa, J.; Gorte, R. J.; White D. *J. Phys. Chem. B* **2000**, *104*, 5124.
(23) Bonn, M.; Brugmans, M. J. P.; Kleyn, A. W.; van Santen, R. A.; Bakker, H. J. *Phys. Rev. Lett.* **1996**, *76*, 2440.
(24) Bonn, M.; Brugmans, M. J. P.; Kleyn, A. W.; van Santen, R. A.; Bakker, *J. Chem. Phys.* **1996**, *105*, 3431.
(25) Vasenkov, S.; Frei, H. J. *J. Am. Chem. Soc.* **1998**, *41*, 207.
(26) Vasenkov, S.; Frei, H. J. *J. Phys. Chem. A* **2000**, *104*, 4327.

(27) Smith, L. J.; Davidson A.; Cheetham, A. K. *Catal. Lett.* **1997**, *49*, 143.
(28) Yuen, L.-T.; Zones, S. I.; Harris, T. V.; Gallegos, E. J.; Auroux, A. *Microporous Mater.* **1994**, *2*, 105.
(29) Troullier, N.; Martins, J. *Phys. Rev. B* **1991**, *43*, 1993.
(30) Perdew, J. P.; Wang, Y. *Phys. Rev. B* **1991**, *45*, 13244.
(31) Shah, R.; Payne, M. C.; Lee, M. H.; Gale, J. D. *Science* **1996**, *271*, 1395.
(32) Shah, R.; Gale, J. D.; Payne, M. C. *Phase Trans.* **1997**, *61*, 67.
(33) Shah, R.; Payne, M. C.; Gale, J. D. *Int. J. Quantum Chem.* **1997**, *61*, 393.
(34) Shah, R.; Gale, J. D.; Payne, M. C. *Chem. Commun.* **1997**, 131.
(35) Stich, I.; Gale, J. D.; Terakura, K.; Payne, M. C. *Chem. Phys. Lett.* **1998**, *283*, 402.
(36) Sandre, E.; Payne, M. C.; Gale, J. D. *Chem. Commun.* **1998**, 2445.
(37) Gale, J. D.; Shah, R.; Payne, M. C.; Stich, I.; Terakura, K. *Catal. Today* **1999**, *50*, 525.
(38) Car, R.; Parrinello, M. *Phys. Rev. Lett.* **1985**, *55*, 2471.
(39) Nosé, S. *J. Chem. Phys*. **1984**, *81*, 511.
(40) Nosé, S. *Mol. Phys.* **1984**, *52*, 255.
(41) Hoover, W. G. *Phys. Rev. A* **1985**, *31*, 1695.
(42) Hutter, J.; Ballone, P.; Bernasconi, P.; Focher, P.; Fois, E.; Goedecker, S.; Parrinello, M.; Tuckerman, M.; CPMD, version 3.0, at MPI fur Festkorperforschung and IBM Zurich Research Laboratory: 1990−1996.
(43) Cook, S. J.; Chakraborty, A. K.; Bell, A. T.; Theodorou, D. N. *J. Phys. Chem*. **1993**, *97*, 6679.
(44) Haw, J. F.; Hall, M. B.; Alvarado-Swaisgood, A. E.; Munson, E. J.; Lin, Z.; Beck, L. W.; Howard, T. *J. Am. Chem. Soc*. **1994**, *116*, 7308.
(45) Barbosa, L. A. M. M.; van Santen, R. A. *J. Catal*. **2000**, *191*, 200.
(46) Blaszkowski, S. R.; van Santen, R. A. *J. Phys. Chem.* **1995**, *99*, 11728.
(47) Kassab, E.; Jessri, H.; Allavena, M.; White, D. *J. Phys. Chem. A* **1999**, *103*, 2766.
(48) Sprik, M.; Ciccotti, G. *J. Chem. Phys*. **1998**, *109*, 7737.
(49) Bolhuis, P. G.; Dellago, C.; Chandler, D. *Faraday Discuss.* **1998**, *110*, 421.
(50) Kofke, T. J. G.; Gorte, R. J.; Farneth, W. E. *J. Catal.* **1988**, *114*, 34.
(51) Kresnawahjuesa, O.; Heussner, R.; Lee, C.-C.; Kuehl, G.; Gorte, R. J. *Appl.Catal. A* **2000**, *199*, 53.
(52) Palkhiwala, A. G.; Gorte, R. J. *Catal. Lett.* **1999**, *51*, 19.
(53) Parrillo, D. J.; Adamo, A. T.; Kokotailo, G. T.; Gorte, R. J. *Appl. Catal.* **1990**, *67*, 107.
(54) Tittensor, J.; Gorte, R. J.; Chapman, D. *J. Catal*. **1992**, *138*, 714.
(55) Lee, C. C.; Gorte, R. J.; Farneth, W. E. *J. Phys. Chem. B* **1997**, *101*, 3811.
(56) Gorte, R. J. *J. Catal.* **1982**, *75*, 164.
(57) Redhead, R. A. *Vacuum* **1962**, *12*, 203.
(58) Parrillo, D. J.; Gorte, R. J. *Catal. Lett*. **1992**, *16*, 17.
(59) Parrillo, D. J.; Gorte, R. J. *Thermochimica Acta* **1998**, *312*, 125.
(60) Kotrla, J.; Kubelkova, L.; Lee, C.-C.; Gorte, R. J. *Journal of Physical Chemistry B* **1998**, *102*, 1437.
(61) Parrillo, D. J.; Lee, C.; Gorte, R. J. *Applied Catalysis A* **1994**, *110*, 67.
(62) Biaglow, A. I., Ph.D. Thesis, University of Pennsylvania, 1993.
(63) Biaglow, A. I.; Gorte, R. J.; Kokotailo, G. T.; White, D. *J. Catal*. **1994**, *148*, 779.
(64) Carduner, K. R.; Villa, M.; White, D. *Rev. Sci. Instrum*. **1984**, *55*, 68.
(65) Tecmag, Houston, TX. 77081.
(66) Murphy, M. D.; Semack, M. G.; White, D. *J. Magn. Reson*. **1987**, *72*, 143.
(67) Šepa, J.; Gorte, R. J.; Suits, B. H.; White, D. *Chem. Phys. Lett.* **1998**, *289*, 281.
(68) Šepa, J., Ph.D. Thesis, University of Pennsylvania, 1998.
(69) Šepa, J.; Gorte, R. J.; White, D.; Suits, B. H.; Swaminathan, V. S. Proceedings of the 12th International Zeolite Conference, 1998, Treacy, M. M. J., Marcus, B. K., Bisher, M. E., Higgins, J. B., Eds.; Materials Research Society: Warrendale, PA, 1998; p. 2287.
(70) Biaglow, A. I.; Gorte, R. J.; White, D. *J. Phys. Chem*. **1993**, *97*, 7135.
(71) Suits, B. H.; Šepa, J.; White, D. *J. Magn. Reson.* **1996**, *A120*, 88.
(72) Wittebort, R. J.; Olenjniczak, E. T.; Griffin, R. G. *J. Chem. Phys*. **1987**, *86*, 541.
(73) Petersen, N. O.; Chan, S. I. *Biochemistry* **1977**, *16*, 2657.; Kohl, J. E.; Semack, M. G.; White, D. *J. Chem. Phys*. **1978**, *69*, 5378.; Wittebort, R. J.; Szabo, A. *J. Chem. Phys*. **1978**, *69*, 1722.
(74) Costain, C. C. *J. Chem. Phys*. **1958**, *29*, 864.